Journal of Applied Polymer Science

Correlation Between Interlamellar Amorphous Structure and Gas Permeability in Poly(lactic acid) Films

Shuichi Sato,[1,2] Tatsuki Nyuui,[3] Go Matsuba,[3] Kazukiyo Nagai[1]

[1]Department of Applied Chemistry, Meiji University, Tama-ku, Kawasaki-shi Kanagawa 214-8571, Japan
[2]Department of Electrical and Electronic Engineering, Tokyo Denki University, Adachi-ku, Tokyo 120-8551, Japan
[3]Department of Polymer Science and Engineering, Yamagata University, Yonezawa Yamagata 992-8510, Japan
Correspondence to: G. Matsuba (E-mail: gmatsuba@yz.yamagata-u.ac.jp)

ABSTRACT: We have investigated the relationship between amorphous structure and its gas permeability of poly(lactic acid) (PLA) using differential scanning calorimetry, wide-angle X-ray scattering, and small-angle X-ray scattering measurements. We focused on the hierarchical interlamellar amorphous structure of various gas-permeable PLA films. The films crystallized just above T_g did not have any long-spacing period peaks at the room temperature even with the existence of crystals; conversely, peaks could be observed from long spacing periods with heating. Therefore, the interlamellar amorphous density became as high as crystalline region one at the room temperature. These high-density amorphous regions, the so-called rigid-amorphous phase, reduced the gas diffusion and permeation. In the case of samples crystallized above 90°C, the long spacing period peaks could be observed even at the room temperature. The amorphous region did not develop the rigid-amorphous phase, and the gas permeability depended only on crystallinity.
 J. Appl. Polym. Sci. **2014**, *131*, 40626.

KEYWORDS: biopolymers and renewable polymers; crystallization; structure–property relations; X-ray

Received 15 January 2014; accepted 21 February 2014
DOI: 10.1002/app.40626

INTRODUCTION

Currently, most polymer composites utilize petroleum-based materials, which are nondegradable, thereby posing significant problems with and incurring substantial cost for disposal. This has motivated significant research in the development of degradable bio-based polymers or green composites. Among these, poly(lactic acid) (PLA) has been widely used as an alternative to petroleum-based polymers.[1–4] Commercially, PLA is prepared by the fermentation of lactic acid produced from natural renewable sources such as corn in a typical compost environment. In fact, the synthesis method is environmentally benign with no emission of carbon dioxide. Although PLA was initially intended for use in biomedical applications, its interesting technological features such as ease of polymer processing, good clarity, and acceptable mechanical properties have widened its use as a material in packaging, electronic, and automobile applications. Furthermore, PLA exhibits carbon dioxide barrier properties, which are highly sought in plastic bottling and food packaging.[5,6] Despite these advantages, the use of PLA remains limited because of its high cost and inferior thermal stability and mechanical properties.

In general, the gas diffusivity, solubility, and permeability of semicrystalline polymers decrease with the degree of crystallinity, X_c.[7] Thus far, several researchers have analyzed and reported the factors affecting the permeability of different polymers. In an earlier study on polyethylene, Michaels and Bixler demonstrated that oxygen permeability decreases with increasing density.[8] This indicates that "denser" crystalline structures are impermeable to small, permeating gas molecules. In other words, the increase in crystallinity decreases the amount of amorphous region that is available for gas absorption. The transport of gas molecules is, therefore, limited to the amorphous phase, in which they need to adopt a tortuous path.

Kanehashi et al. published a review based on an extensive literature survey in which they discussed the relationship between the X_c and the gas permeability of a many semicrystalline and liquid crystalline polymers.[9] The review stated that the gas diffusivity, solubility, and permeability decrease with increasing crystallinity in many polymers, while it highlighted that some polymers exhibited almost constant or slightly increased values of permeability and diffusivity at lower X_c values. Furthermore, at higher X_c values, the gas permeability and diffusivity essentially decreased. At

Additional Supporting Information may be found in the online version of this article.

the same time, solubility decreased with increasing X_c. These results indicate an unsolved problem pertaining to the inconsistency between gas permeability (diffusivity and solubility) and X_c. This is crucial because X_c is not a good parameter to describe as complicated crystal/amorphous structures.

Bao et al. [10] have reported the gas permeability of amorphous PLA films by estimating the gas diffusivities and solubilities using a time-lag method. It was found that the diffusivities increased with the annealing temperature, while the solubilities decreased. Colomines et al.[5] have observed that oxygen permeability was independent of the X_c of PLA. Moreover, Driesken et al.[11] have shown that an increase X_c causes a decrease in oxygen permeability, but it is not in linear proportion to the decrease in amorphous volume. Sawada et al.[12] have reported oxygen permeability of up to 20% for PLA membranes because of the decreased continuous space around crystalline regions, which was due to the stress imposed on macromolecular chains at the interface of lamellar crystals. Later, Guinault et al.[13] analyzed the helium and oxygen barrier properties of PLA films as a function of stereochemistry and X_c. According to those authors, gas permeability increased with increasing amounts of α'-form crystals,[14] which were specifically observed under low crystallization temperature conditions. Furthermore, it has been reported that the gas barrier properties could be improved by increasing the formation of α-form crystals with higher temperature crystallization. In addition, they also insisted that gas permeability (or barrier properties) did not strongly depend on X_c but rather depended on the amount of rigid-amorphous region. Furthermore, under high-pressure conditions, Oliveila et al.[15,16] studied the gas solubility of carbon dioxide in PLA films under several annealing conditions and L : D contents. They found that the experimental data could be described by the dual sorption model. The solubility strongly depended on the L : D contents. The crystals in PLA films affect the gas solubility.

PLA crystals have been extensively studied based on the morphology of the crystalline structure and the influence of nucleating agents. Conventionally, PLA crystallizes in the α-form. However, in the case of crystallization below 90°C, Kawai et al. observed precise crystal structure and crystallization processes of PLA in the α'-form, which is a distorted α-form.[14] In amorphous region, many researchers have reported physical aging during annealing below T_g.[17–21] Mano et al. have studied both crystalline and amorphous forms of PLA by differential scanning calorimetry (DSC) measurements to investigate both molecular dynamics and structural relaxation.[22] They observed the mobility of amorphous chains in semicrystalline PLA with confinement on segmental mobility of the interlamellar structure.

Despite the extensive research and substantial data reported so far, the correlation between lamellar/interlamellar structure and gas transport properties still remains unclear. It is extremely important to clarify the role of crystalline/amorphous structure in improving and controlling gas transport properties. Therefore, the aim of this study is to understand the nanometer-scale hierarchies of crystal and amorphous structures influencing the gas transport properties of PLA films, in which the morphology is modified by crystallization from glassy samples at various temperatures.

EXPERIMENTAL

Materials

PLA polymer (4032D) was purchased from NatureWorks LLC, Minnetonka, MN. The ratio of isomers was in the L : D range of 96.0 : 4.0–96.8 : 3.2. PLA films were casted from a 2 wt % solution in dichloromethane using flat-bottomed glass Petri dishes in a glass bell-type vessel. The solvent was slowly evaporated for 48 h under atmospheric pressure at room temperature. Next, the dried PLA films were vacuum-crystallized at 70, 80, 90, and 150°C for 48 h, and the corresponding samples were denoted PLA-70, PLA-80, PLA-90, and PLA-150, respectively. The crystallization of the samples was carried out to completely eliminate any residual solvent and to obtain films with various X_c values. The thickness of the obtained films was between 35 and 45 μm. We confirmed the chemical structure and the removal of solvent by proton nuclear magnetic resonance (JNM-ECA500, JEOL Ltd., Tokyo, Japan) and Fourier-transform infrared spectroscopy (FT-IR 460+, JASCO CO., Tokyo, Japan). Further details on the samples have been reported elsewhere by Sawada et al.[12]

Characterization

The thermal properties of the prepared PLA films were analyzed using a Q-200 system DSC (TA Instruments, New Castle, DE). The correlation between PLA film structure and gas transport properties was investigated by analyzing the first heating scan data after annealing. The heating rate was kept at 5°C/min under nitrogen atmosphere. From these data, the degree of crystallinity, X_c, was determined as follows:

$$X_c = \frac{\Delta H_m - \Delta H_c}{\Delta H_m^0} \quad (1)$$

where ΔH_m and ΔH_c are the enthalpies of melting and crystallization of a polymer, respectively, and ΔH_m^0 is the enthalpy of a perfect PLA crystal, which is 93 J/g.[23]

Small-angle X-ray scattering (SAXS) measurements were performed with a Nano-viewer (Rigaku Co., Tokyo, Japan) using a Cu-Kα radiation source. The wavelength of the X-ray beam used was 0.154 nm, and the scattered X-rays were detected by a 2D detector (Pilatus 100K; Detris, Baden, Switzerland). The scattering vector, q, was recorded between 0.1 and 1.0 nm^{-1}, where q is given by $q = 4\pi\sin\theta/\lambda$ (2θ is the scattering angle).

Wide-angle X-ray scattering (WAXS) measurements were carried out on a Rint Rapid X-ray diffractometer (Rigaku, Co., Tokyo, Japan) using a Cu-Kα radiation source. The wavelength of the X-ray beam was 0.154 nm. The WAXS intensities were detected by a curved imaging plate. The q range covered in the WAXS experiments was between 2.5 and 25 nm^{-1}.

RESULTS AND DISCUSSIONS

Gas Transport Properties

The gas permeability, diffusion, and solubility coefficients at 35°C of the PLA films have been discussed in previous papers.[12] The Supporting Information describes the conditions and results of the gas permeability data in detail. The solubility coefficients of O_2, N_2, CO_2, and CH_4 decreased monotonically with increasing crystallization temperature, PLA-70 > PLA-80 > PLA-90 > PLA-150. Conversely, the gas permeability and diffusion

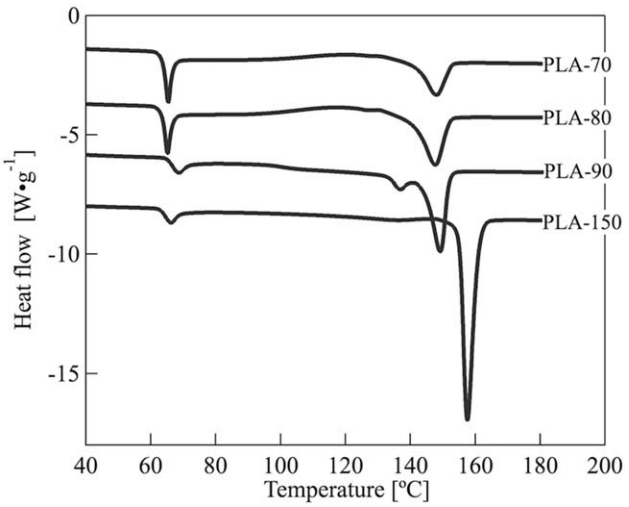

Figure 1. DSC thermograms of PLA films after annealing at 70, 80, 90, and 150°C (PLA-70, PLA-80, PLA-90, and PLA-150, respectively). The heating rate was kept at 5°C/min.

constants of O_2, N_2, CO_2, and CH_4 had different tendencies from that of the solubility with PLA-80 > PLA-90 > PLA-70 > PLA-150. These results suggest that the gas permeability of PLA films depends more on the diffusivity than on the solubility.

DSC Measurements

The thermal properties of the PLA films after annealing at 70, 80, 90, and 150°C (PLA-70, PLA-80, PLA-90, and PLA-150, respectively) were analyzed as shown in Figure 1. From the thermograms, the glass transition peak, crystallization peak, and melting peak of the PLA crystals were observed at ~63, 118, and 140–160°C, respectively. The corresponding thermal properties are summarized in Table I. Here, with multiple melting peaks, the melting temperature (T_m) was defined as the temperature at which the corresponding maximum peak occurs. For the PLA films PLA-70 and PLA-80, we observed broad crystallization peaks, while no crystallization peaks were observed for the PLA-90 and PLA-150 films because the X_c is high enough after crystallization. The X_c value was found to increase with increasing in crystallization temperature: PLA-150 > PLA-90 > PLA-80 > PLA-70. Furthermore, in the case of PLA-150, the melting temperature was found to be higher than those of PLA-70, PLA-80, and PLA-90. Because PLA-70 and PLA-80 films exhibited broad exothermic peaks corresponding to the crystallization of the films, they exhibited high X_c below 10%.

In the PLA-70 and PLA-80 films, we observed strong endothermic peaks around the glass transition temperature, T_g. Conversely, the PLA-90 and PLA-150 sample showed weak endothermic peaks. Pan et al. performed DSC measurements of amorphous PLA films obtained by annealing at tempeartures below T_g.[19] According to their study, the endothermic peak around T_g increased with annealing time. Similarly, Mano et al. analyzed the effect of X_c on these endothermic peaks in PLA films.[22] Their study indicates that these endothermic peaks could be attributed to the physical aging of PLA films. These physical aging processes were observed in β-form polypropylene[20] and polysulfone films[21]. The physical aging is the process of approaching an equilibrium state that is undergone by a glass held in constant environmental conditions after its formation history. Furthermore, Iannace and Nicolais studied the isothermal chain mobility of crystalline PLA films with DSC measurements.[24] From the heat capacity analysis, the fraction of rigid-amorphous phase, in which the relaxation process does not occur even above T_g, was observed during the crystallization process. Therefore, in our results, in the cases of PLA-70 and PLA-80, the amorphous chains could enter a nonequilibrium state, that is, the rigid-amorphous phase. This happens through a rearrangement of polymer chains from the nonequilibrium state to molten-type morphology by a microstructural evolution such as conformational change. In the case of the PLA-150 films, the crystallization temperature is high enough that the amorphous chains might be in the equilibrium state.

WAXS Measurements

The crystallinity of the PLA films was estimated by WAXS. Figure 2 shows the WAXS profiles of annealed PLA films. According to previous peak attribution,[25] the peaks at $q = 8.5$ and 21.0 nm^{-1} are those of stereocomplex crystals due to diffraction from the (110), and (300)/(030) planes, respectively, while the peaks at $q = 11.3$ and 13.1 nm^{-1} are those of PLA crystals due to the diffraction from the (110)/(200) and (113)/(203) planes, respectively. We observed crystalline peaks in all PLA films, which increased in the intensity with increasing crystallization temperature. From Figure 3, we evaluated the d-spacing of the (110)/(200) plane and the crystal size $B_{110/200}$ using the Scherrer equation as follows:

$$B_{110/200} = \frac{K\lambda}{\beta \cos\theta} \quad (2)$$

where K is a dimensionless shape factor with a value close to unity (=0.9), and β is the line broadening at half the maximum intensity in radians.[26] It was observed that the d-spacing decreased with increasing crystallization temperature. This

Table I. Thermodynamic Parameters of the Poly(Lactic Acid) (Pla) Films Obtained After Annealing at 70, 80, 90, and 150°C (PLA–70, PLA–80, PLA–90, and PLA–150, respectively).

	T_g [°C]	T_c [°C]	ΔH_c [J/g]	T_m [°C]	ΔH_m [J/g]	X_c [%]
PLA-70	63.6	120.2	10.7	148.1	11.2	0.53
PLA-80	63.4	117.1	9.7	147.8	16.9	7.81
PLA-90	65.2	-	-	149.2	21.9	23.5
PLA-150	63.0	-	-	157.6	36.7	39.5

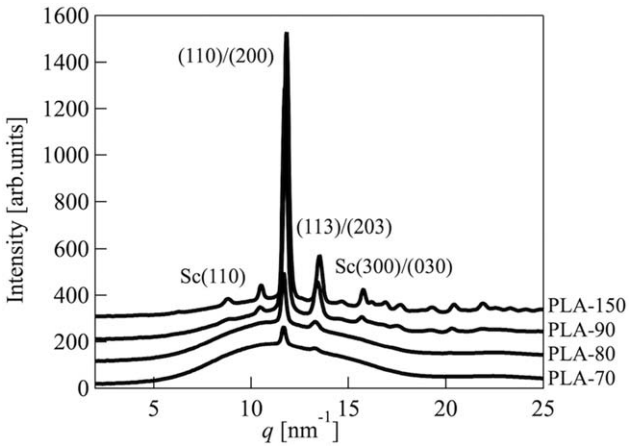

Figure 2. WAXS profiles of the PLA films annealed at different temperature.

decrease could be attributed to the transition from the α' crystalline state at low temperatures to the α crystalline state above 120°C.[14] Therefore, it could be assumed that the crystal form of the PLA-70, PLA-80, and PLA-90 samples is the α'-form, while that of PLA-150 is the α-form. This transformation in the crystal structure is consistent with the T_m changes observed from the DSC measurements in Figure 1. In the WAXS patterns, it was observed that the diffraction intensity was PLA-150 > PLA-90 > PLA-80 > PLA-70. This tendency is consistent to increasing with increasing crystallization temperature due to increased X_c. Furthermore, the crystallite size also increases with crystallization temperature because of shallow quenching depth. These results signify that the size, crystal form, and X_c are not the key parameters influencing the gas permeability and diffusivity. However, the solubility coefficients of the gas molecules correlated strongly with X_c because of the reduction of the amorphous volume that could be used for the penetrant to make a diffusional jump and avoid the swelling of gas molecules. Next, we focused on the amorphous structure at the 10 nm scale.

SAXS Measurements

Figure 4 shows the SAXS profiles of the PLA-70, PLA-80, PLA-90, and PLA-150 samples recorded at room temperature. For

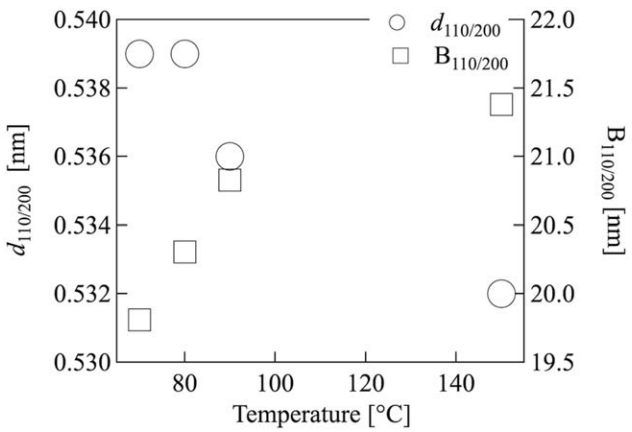

Figure 3. Annealing temperature dependence of *d*-spacing of (110)/(200) plane and crystalline size $B_{110/200}$.

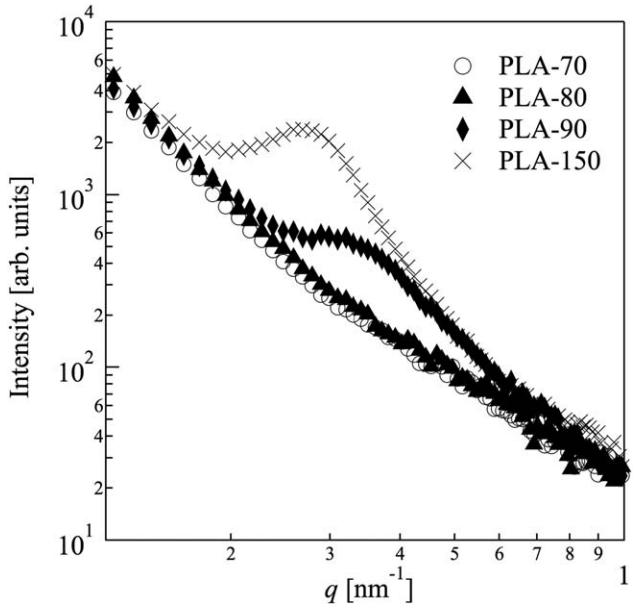

Figure 4. SAXS profiles of PLA films annealed at different temperatures.

the PLA-90 and PLA-150 samples, the SAXS patterns indicated a clear peak due to the long spacing period. The peak position moves to smaller q with increasing crystallization temperature. From the SAXS profiles of PLA-90 and PLA-150, the lengths of the long spacing periods were estimated to be 20.1 and 27.3 nm, respectively. In general, the long spacing period depended quite strongly on the crystallization temperature. The lamellar crystal thickness decreased with the quenching depth. Furthermore, the peak intensity increased with crystallization temperature due to the increase in X_c.

Meanwhile, in the PLA-70 and PLA-80 samples, we did not observe any peaks due to long spacing periods. Conversely, crystals were observed with WAXS and DSC measurements. The lack of scattering from long spacing periods might be caused not by lamellar structure but rather by fringed-micelle-type structure. To precisely clarify the formation of 10-nm scale structure in PLA-70 and PLA-80, we performed SAXS measurements (Figure 5) at 80°C and at room temperature. There was no crystal growth during the heating process because the samples were annealed for a short time of 10 min. In the SAXS profile recorded at 80°C, we observed the hidden scattering peak originating from the lamellar structure. The corresponding long spacing periods were estimated to be 17.9 and 19.0 nm for PLA-70 and PLA-80, respectively. The hidden long spacing periods also increased with crystallization temperature. Furthermore, on cooling the samples from 80°C to room temperature, the SAXS profiles did not show any scattering peaks indicates that the samples regained their original structure. These results indicate the absence of lamellar crystals at room temperature but signify minute density fluctuations on the order of 10 nm from the lamellar crystals. The density of the amorphous region in PLA-70 and PLA-80 is roughly the same as that of the crystalline region at room temperature. In other words, the rigid-amorphous phase exists between the lamellar crystals. When the sample is annealed above T_g, the molecular motion becomes

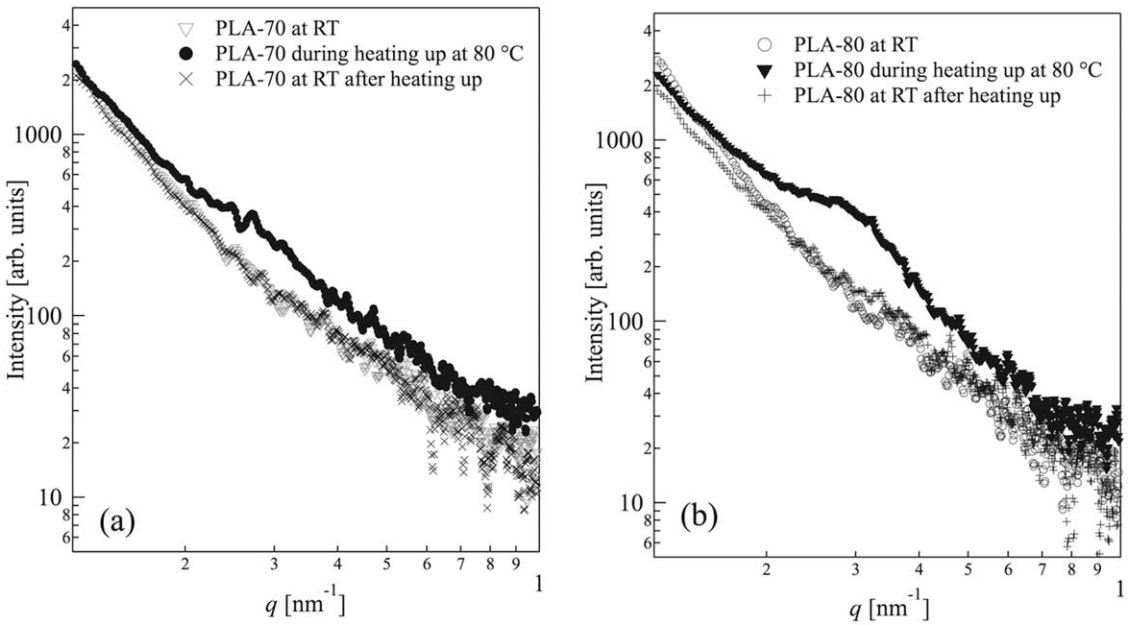

Figure 5. SAXS profiles of PLA films measured at room temperature (RT) and 80°C. (a) PLA-70 and (b) PLA-80.

active, especially in the rigid-amorphous phase. Therefore, density fluctuations from the lamellar structure could be detected. These findings suggest that amorphous state of the interlamellar region might depend strongly on the permeability of gas molecules.

Correlation Between the Rigid-Amorphous Phase and the Gas Permeability

Figure 6 shows the lamellar and interlamellar amorphous structure in the case of various annealing temperature conditions. The rigid-amorphous phase exists in PLA-70 and PLA-80 because of the lack of scattering peaks in the SAXS measurements. In the DSC measurements, strong endothermic peaks were observed around T_g because of the physical aging of amorphous polymer chains. Conversely, in the PLA-90 and PLA-150 films, we observed the SAXS peak from long spacing periods and weak endothermic peaks around T_g. The samples crystallized above 90°C were relaxed because the rigid-amorphous phase decreases with crystallization temperature.[24]

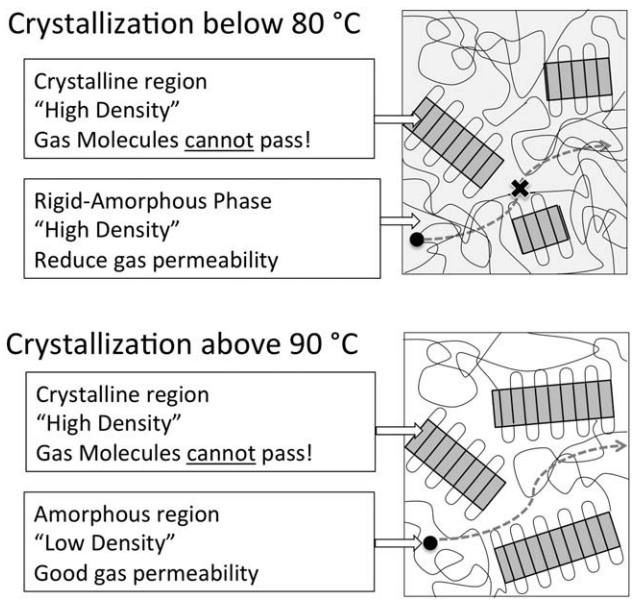

Figure 6. The schematic drawing of lamellar crystals and interlamellar amorphous structure in various annealing temperature conditions.

Generally speaking, the gas permeability, diffusivity and solubility depend on X_c.[7] This is especially true for the gas solubility of PLA films because the dissolution of gas molecules in the films depends on the amorphous fraction ($=1-X_c/100$). However, for the gas diffusivity and the gas permeability (PLA-80 > PLA-90 > PLA-70 > PLA-150), the tendencies are quite different from that of X_c (PLA-150 > PLA-90 > PLA-80 > PLA-70). We focused on the correlation between the gas permeability (gas diffusivity) and the rigid-amorphous phase. Tsujita et al. have reported that the permeability of amorphous polymers decreased upon annealing below T_g.[27,28] The reduction of gas permeability could be due to the restriction of chain mobility in the rigid-amorphous phase; in other words, due to the decrease of free volume in glassy polymeric membranes.[29] The rigid-amorphous phase restricts the diffusion of gas molecules quite strongly. This consideration is again consistent with the SAXS results, which indicate an increase in the density of the amorphous region with increasing annealing temperature. The effects of the restriction became weaker at higher crystallization temperatures because of decreases in the fraction of the rigid-amorphous phase.[24] In particular, the gas diffusivity and the gas permeability of the PLA films depended on both the existence of rigid-amorphous phase and X_c. In PLA-70, PLA-80, and PLA-90, X_c is very small, but the effect of the rigid-amorphous phase is quite large. Consequently, the gas permeability

increased with crystallization temperature because of the decreased fraction of rigid-amorphous phase. Conversely, in PLA-90 and PLA-150, the gas permeability decreased with increasing crystallization temperature because X_c became the main factor by reducing the rigid-amorphous phase.

CONCLUSIONS

In summary, we have analyzed the relationship between the amorphous structure of PLA films and gas permeability. It was found that the crystallite size and crystallinity increased with increasing annealing temperature. However, the abovementioned parameters are not the sole influences on the gas permeability of PLA films because not only do crystallinity and crystal structure have strong dependence on crystallization temperature, but amorphous structure does as well. DSC measurements indicated the occurrence of physical aging processes, especially in the case of samples annealed below 80°C. The amorphous region in these PLA films might transform into the so-called rigid-amorphous phase. This fraction decreases with crystallization temperature, according to the DSC results. The density of the rigid-amorphous phase is roughly the same as that of lamellar crystals according to SAXS measurements. This implies that the high-density and low mobility of the rigid-amorphous phase restricted the gas diffusion and permeation in the PLA films. Conversely, in PLA films annealed above 90°C, the amorphous region did not develop rigid-amorphous and condensed phase properties. In these cases, the gas molecules could penetrate the amorphous region and/or between the lamellar crystals and amorphous region. Then the gas permeability and the gas diffusivity depended on the amount of amorphous region such as the solubility of gas molecules.

REFERENCES

1. Auras, R. A.; Lim, L. T.; Selke, S. E. M.; Tsuji, H. Poly(lactic acid): Synthesis, Structures, Properties, Processing, and Applications; John Wiley & Sons, New York, NY, **2010**.
2. Okihara, T.; Tsuji, M.; Kawaguchi, A.; Katayama, K.; Tsuji, H.; Hyon, S. H.; Ikada, Y. *J. Macromol. Sci.Phys.* **1991**, 119.
3. Iwata, T.; Doi, Y. *Macromol. Chem. Phys.* **1999**, *200*, 2429.
4. Urayama, H.; Kanamori, T.; Fukushima, K.; Kimura, Y. *Polymer* **2003**, *44*, 5635.
5. Colomines, G.; Ducruet, V.; Courgneau, C.; Guinault, A.; Domenek, S. *Polym. Int.* **2010**, *59*, 818.
6. Auras, R.; Harte, B.; Selke, S. *Macromol. Biosci.* **2004**, *4*, 835.
7. Paul, D. R.; Yampol'skiĭ, Y. P. Polymeric Gas Separation Membranes; C R C Press LLC, Boca Raton, FL, **1994**.
8. Michaels, A. S.; Bixler, H. J. *J. Polym. Sci.* **1961**, *50*, 393.
9. Kanehashi, S.; Kusakabe, A.; Sato, S.; Nagai, K. *J. Membr. Sci.* **2010**, *365*, 40.
10. Bao, L.; Dorgan, J. R.; Knauss, D.; Hait, S.; Oliveira, N. S.; Maruccho, I. M. *J. Membr. Sci.* **2006**, *285*, 166.
11. Drieskens, M.; Peeters, R.; Mullens, J.; Franco, D.; Lemstra, P. J.; Hristova-Bogaerds, D. G. *J. Polym. Sci. B Poly. Phys.* **2009**, *47*, 2247.
12. Sawada, H.; Takahashi, Y.; Miyata, S.; Kanehashi, S.; Sato, S.; Nagai, K. *Trans. Mater. Res. Soc. Jpn.* **2010**, *35*, 241.
13. Guinault, A.; Sollogoub, C.; Ducruet, V.; Domenek, S. *Eur. Polym. J.* **2012**, *48*, 779.
14. Kawai, T.; Rahman, N.; Matsuba, G.; Nishida, K.; Kanaya, T.; Nakano, M.; Okamoto, H.; Kawada, J.; Usuki, A.; Honma, N.; Nakajima, K.; Matsuda, M. *Macromolecules* **2007**, *40*, 9463.
15. Oliveira, N. S.; Dorgan, J.; Coutinho, J. A. P.; Ferreira, A.; Daridon, J. L.; Marrucho, I. M. *J. Poly. Sci. Part B: Polym. Phys.* **2007**, *45*, 616.
16. Oliveira, N. S.; Dorgan, J.; Coutinho, J. A. P.; Ferreira, A.; Daridon, J. L.; Marrucho, I. M. *J. Poly. Sci. Part B: Polym. Phys.* **2006**, *44*, 1010.
17. Tsuji, H.; Tsuruno, T. *Macromol. Mater. Eng.* **2010**, *295*, 709.
18. Acioli-Moura, R.; Sun, X. S. *Polym. Eng. Sci.* **2008**, *48*, 829.
19. Pan, P.; Zhu, B.; Inoue, Y. *Macromolecules* **2007**, *40*, 9664.
20. Bai, H.; Luo, F.; Zhou, T.; Deng, H.; Wang, K.; Fu, Q. *Polymer* **2011**, *52*, 2351.
21. Murphy, T. M.; Langhe, D. S.; Ponting, M.; Baer, E.; Freeman, B. D.; Paul, D. R. *Polymer* **2012**, *53*, 4002.
22. Mano, J. F.; Gómez Ribelles, J. L.; Alves, N. M.; Salmerón Sanchez, M. *Polymer* **2005**, *46*, 8258.
23. Fischer, E. W.; Sterzel, H.; Wegner, G. *Kolloid-Z.u.Z.Polymere.* **1973**, *251*, 980.
24. Iannace, S.; Nicolais, L. *J. Appl. Polym. Sci.* **1997**, *64*, 911.
25. Rahman, N.; Kawai, T.; Matsuba, G.; Nishida, K.; Kanaya, T.; Watanabe, H.; Okamoto, H.; Kato, M.; Usuki, A.; Matsuda, M.; Nakajima, K.; Honma, N. *Macromolecules* **2009**, *42*, 4739.
26. Jenkins, R.; Snyder, R. L. Introduction to X-ray Powder Diffractometry, John Wiley & Sons, New York, NY, **1996**; p 355.
27. Hachisuka, H.; Tsujita, Y.; Takizawa, A.; Kinoshita, T. *Polymer* **1988**, *29*, 2050.
28. Tsujita, Y. *Prog. Polym. Sci.* **2003**, *28*, 1377.
29. Kobayashi, Y.; Zheng, W.; Meyer, E. F.; McGervey, J. D.; Jamieson, A. M.; Simha, R. *Macromolecules* **1989**, *22*, 2302.